Modeling of Memory Effects in Nanofluidic Diodes

Javier Cervera,[1,a)] Sergio Portillo,[1] Patricio Ramirez,[2] and Salvador Mafe[1]

[1]*Dept. de Física de la Terra i Termodinàmica, Universitat de València, E-46100 Burjassot, Spain*
[2]*Dept. de Física Aplicada, Universitat Politècnica de València, E-46022 València, Spain*

a) Author to whom correspondence should be addressed: jcervera@uv.es

ABSTRACT

Nanofluidic diodes and ionic solutions find application in electrochemical circuits for information processing, controlled release, and signal conversion in hybrid devices. Here, we describe a physical model that accounts for the memory effects observed in conical nanopores in terms of the driving signal and ionic solution characteristics. The concepts invoked describe the device operation on the basis of the electrical interaction between the pore surface charges and the nanoconfined ionic solution. The physical insights provided can explain the experimental dependence of the nanofluidic tunability on the amplitude and frequency of the driving signal, the ionic concentration, and the solution pH. The model should also be useful for the design of electrochemical circuits based on ionic conduction in asymmetric memristors.

I. INTRODUCTION

Memory effects and memristors based on ionic conduction are of broad interest in the fundamental and applied physics of fluids because they constitute the core of neuromorphic information processing.[1-6] As devices and experimental data accumulate, there is a clear need to develop physical models that describe the basic phenomenology observed in terms of fundamental concepts.[3,7,8] We have experimentally demonstrated a membrane memristor based on an array of nanofluidic conical pores functionalized on a polymeric substrate.[6] The operation of this electrochemical memory resistor is based on the electrical interaction between the pore surface charges and the nanoconfined ionic solution.[9-11]

We explore here a theoretical model that allows a description of the experimental data on the basis of physics concepts that should be of broad interest to nanofluidic memristors. The model can explain the nanofluidic tunability in terms of the amplitude and frequency of the driving signal, the ionic concentration, and the solution pH.[6] The theoretical description of biomimetic ionic conductors[2,4,11] is also relevant to ion channel biophysics[12] and can be useful for the understanding of sensors and actuators in hybrid bioengineering circuits[1,5,11] and plant physiology.[13]

Previous models that make use of general concepts relevant to our problem concerned finite-element calculations and analytical approximations for memory effects in conical microfluidic pores.[7] In Ref. 7, a proposal consisting of an iontronic circuit with micrometer cones simulating sodium and potassium channels was also given. Also, new experiments and models have demonstrated memory effects in aqueous electrolytes and sub-nanoscale channels, where theoretical emphasis was made on the coupling of ion transport with interfacial processes and biomimetic neuromorphic computations.[3]Action potentials upon a pulse stimulus and a spike train upon a sustained stimulus were also reported. In addition, analytical models for

memristive relaxation equations relevant to plant electrophysiology were experimentally checked in Ref. 13.

Here, the specific problems addressed are:

i) the description of the ionic conduction characteristics of negatively-charged conical nanofluidic diodes, with emphasis on the memory and current rectification effects, in terms of a simple analytical model that incorporates directly accessible physico-chemical magnitudes. The modeling equations can be extended further to other ionic transport phenomena and should also attract interest for the design of electrochemical logic functions and memory circuits; and

ii) the validation of the model assumptions using a comprehensive set of experimental data that include not only the physical characteristics of the electrical driving signal but also the chemical properties of the electrolyte solution.

II. RESULTS AND DISCUSSION

Figures 1(a)–1(d) show the observed current (I)–voltage (V) curves for different values of the frequency f and amplitude V_0 of the applied voltage $V(t) = V_0 \sin(2\pi ft)$, where t is the time, the ionic concentrations, and the cation type. The multipore membrane is a 12.5-μm thick polyimide (PI) foil irradiated by swift heavy ions whose ion tracks are converted into conical nanopores by asymmetric track-etching.[6] The PI samples are irradiated, leading to the formation of latent ion tracks. SEM images and electrical conductance measurements suggest pore radii of the order of 10 nm (cone tip) and 100 nm (cone base). The ionization of the carboxylate residues on the pore surface gives the pH-dependent pore charges. For a neutral pH, surface charge densities in the range between −0.1 and −1.0 e/nm^2, where e is the elementary charge, are obtained.[6] The membrane area exposed to the salt solutions is 1 cm^2 approximately.

Ag|AgCl electrodes with 2M KCl solution salt bridges are used to control the input voltages (V) and output currents (I) with a BioLogic SP-200 potentiostat.

At low enough frequency (0.01 Hz in Fig. 1(a)), a steady-state I–V curve with no hysteresis is obtained because the time that characterizes the relaxation process of the mobile ions within the pore is much lower than the period of the driving signal. The conical pores show rectifying currents due to the nanostructure asymmetry: a low resistance is observed when the current enters the tip while a high resistance is obtained when it enters the cone base.[9]

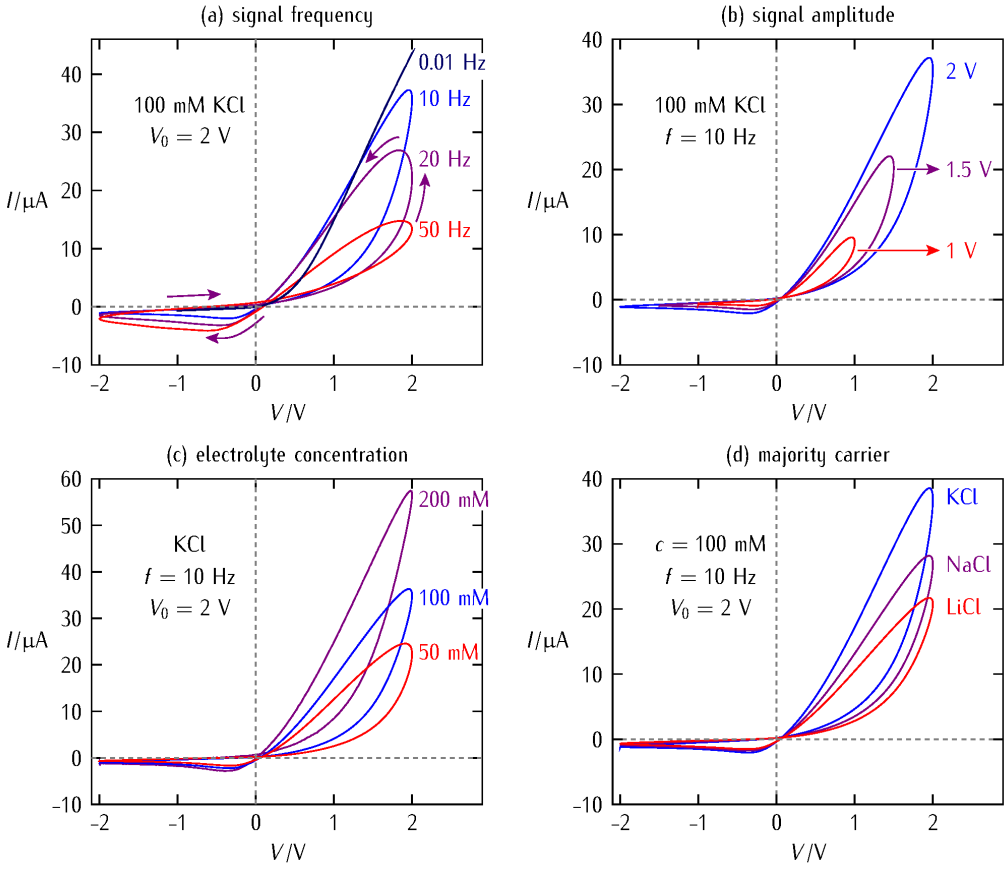

FIG. 1. (a) Experimental I–V curves obtained for different frequencies f of the applied sinusoidal signal. The amplitude is $V_0 = 2$ V and the solution concentration is $c = 100$ mM KCl. The arrows show the time evolution of the output current. (b) I–V curves for distinct V_0, with $f = 10$ Hz and $c = 100$ mM KCl. (c) I–V curves for different concentrations c, with $V_0 = 2$ V and $f = 10$ Hz. (d) I–V curves for $c = 100$ mM LiCl, NaCl, and KCl solutions, with $V_0 = 2$ V and $f =$

10 Hz. Reproduced with permission from J. Phys. Chem. Lett. 14, 10930 (2023). Copyright 2023 American Chemical Society.

For signal frequencies f in the range 10–50 Hz, memory effects are clearly observed (Fig. 1(a)). The conical pore hysteresis is more significant for $V > 0$ than for $V < 0$ because the mobile ions accumulate at the pore tip in the first case while they are depleted in the second case.[9] At too high frequencies, however, the ions cannot follow the rapid changes of the external driving signal and both the rectification and memory characteristics are gradually lost (Fig. 1(a)). The current can also be modulated by the voltage amplitude (Fig. 1(b)), the ionic concentration (Fig. 1(c)), and the cation type (Fig. 1(d)).[6] Note that the solution concentration dictates the availability of electrical carriers and modulates also the Debye screening of the pore surface charges in Fig. 1(c).[9] The cation mobility series $Li^+ < Na^+ < K^+$ is in agreement with the currents observed in Fig. 1(d).[6] The above experimental facts show clear memristive characteristics[14,15] and are reminiscent of biomimetic pores and biological ion channels.[12]

We explore now a simple theoretical model that can provide a qualitative description of the experimental curves of Fig. 1. While the approximately conical pore geometry does not change with time, the ionic pore solution concentrations do change following the external driving signals. The electric current is mostly transported by counterions and, in the pore solution, conduction dominates over diffusion for these ions. Hence, the flux density of the counterions can be approximated by $J_i = z_i c_i D(F/RT)E$, where z_i and c_i are the charge number and concentration of the counterions, D is the diffusion coefficient, F is the Faraday constant, R is the gas constant, T is the temperature, and E is the axial electric field.

The time relaxation of the pore conductance should follow that of the counterion concentration, which could be regarded as the state variable here. The time relaxation of the

counterion concentration in the pore solution when a constant electric field (V_0/L) is applied across the membrane thickness L must satisfy the continuity equation at axial position x:

$$\frac{\partial c_i}{\partial t} = -\frac{\partial J_i}{\partial x} \rightarrow \begin{cases} X_+ / \tau_{+0} \approx \dfrac{F}{RT} Dc \dfrac{(V_0/L)}{L} \\ X_- / \tau_{-0} \approx \dfrac{F}{RT} Dc \dfrac{(V_0/L)}{L} \end{cases} \quad (1)$$

where the relaxation times τ_{+0} and τ_{-0} characterize the changes in the pore ionic concentrations. Note that the counterion, which is the cation for a negatively-charged pore, has concentrations that are of the order of magnitude of the fixed charge concentrations X_+ (*tip*) and X_-(*base*), respectively. The conical pore asymmetry responsible for the current rectification is explicitly introduced by considering the cases where the counterions enter the nanopore from the tip and from the base.[9] We refer to the case when the applied voltage is positive and the cations enter the pore tip from the left solution of ionic concentration c with the subscript j = +. We refer to the case when the applied voltage is negative and the cations enter the pore base from the right solution of ionic concentration c with the subscript subscript j =– .

In Eq. (1), the different relaxation times τ_{+0} and τ_{-0} arise from the distinct physical characteristics of the cone tip and base solutions. In these solutions, the counterion concentrations are of the order of magnitude of X_+ (*tip*) and X_-(*base*), respectively. This approximation has clear experimental grounds because of the local electroneutrality condition and the fact that the cation is the majority carrier; see Figs. 2 and 3 of Ref. 9. Note also that the ratio X_+ / X_- follows the pore radii ratio $a_-(base)/a_+(tip) \approx 10-100$ because $X_j = 2|\sigma|/(Fa_j)$ and the surface charge density σ is approximately constant.[9]

The approximation of Eq. (1) should be qualitatively valid and explicitly introduces the conical pore asymmetry responsible for the current rectification.[9] The conical pore relaxation is

thus characterized by two different times for the tip and base ionic solutions whose orders of magnitude are:

$$\tau_{+0} \approx \frac{X_{+}\left(L^2/D\right)}{cFV_0/(RT)}$$
$$\tau_{-0} \approx \frac{X_{-}\left(L^2/D\right)}{cFV_0/(RT)} \qquad (2)$$

These different relaxation processes for the ionic concentrations should give distinct relaxation times for the pore conductances $G_j(t)$ (j = +,–) following the externally applied driving signal:[7,13]

$$\frac{\mathrm{d}G_j(t)}{\mathrm{d}t} = -\frac{\left[G_j(t) - G_j^{\mathrm{f}}\right]}{\tau_j}, \quad j = +,- \qquad (3)$$

where G_j^{f} are the limiting final values of the conductances of Fig. 1 and the frequencies $f_j = 1/\tau_j$ characterize now the pore response when driven by sinusoidal voltage signals $V(t) > 0$ (j = +) and $V(t) < 0$ (j = –), respectively. Thus, the frequencies f_j of Eq. (3) are not equal to the frequencies $f_{j0} = 1/\tau_{j0}$ of Eq. (2), because a time-dependent signal $V(t) = V_0 \sin(2\pi ft)$ of frequency f rather than a constant voltage V_0 of Eq. (1) is applied. In this case, the external voltage oscillates between V_0 and $-V_0$ and the system response (f_+ and f_-) should depend on *both* f_{+0} and f_{-0} and the driving frequency f.

Because no memory effects are observed in the zero frequency limit of the external driving signal (Fig. 1(a)),[6,13] we can change V_0 for $V(t)$ in Eq. (2) to obtain the finite frequencies f_j of Eq. (3), and integrate over time the resulting equation to obtain:

$$G_+(t) \approx G_+^{\mathrm{f}} + (G_+^{\mathrm{i}} - G_+^{\mathrm{f}}) \exp\left\{ -\frac{f_{+0}}{2\pi f}\left[1-\cos(2\pi f t)\right] \right\},\ 0 < t < 1/2f$$
$$G_-(t) \approx G_-^{\mathrm{f}} + (G_-^{\mathrm{i}} - G_-^{\mathrm{f}}) \exp\left\{ -\frac{f_{-0}}{2\pi f}\left[1+\cos(2\pi f t)\right] \right\},\ 1/2f < t < 1/f \qquad (4)$$

where G_j^{i} are the initial values of the conductances in Fig. 1 for sinusoidal signals $V(t) > 0$ (j = +) and $V(t) < 0$ (j = –), respectively. Note the *qualitative* nature of Eq. (4), which is obtained from the Eqs. (1)–(3), and allows only order of magnitude estimations for the frequencies f_j (j =+,–). Equation (4) implicitly assumes that when the electric potential $V(t)$ changes, the conductances $G_j(t)$ can follow these changes only after a delay time.[13]

From Eq. (4), the currents $I_j(t) = G_j(t)V(t)$ (j = +,–) are:

$$I_+(t)/I_0 = \left\{ 1 + (r-1)\exp\left\{ -\frac{f_{+0}}{2\pi f}\left[1-\cos(2\pi f t)\right] \right\} \right\} \sin(2\pi f t),\ 0 < t < 1/2f,\ V(t) > 0$$
$$I_-(t)/I_0 = \left\{ r - (r-1)\exp\left\{ -\frac{f_{-0}}{2\pi f}\left[1+\cos(2\pi f t)\right] \right\} \right\} \sin(2\pi f t),\ 1/2f < t < 1/f,\ V(t) < 0 \qquad (5)$$

where $I_0 = G_0 V_0$ is a reference current obtained for the generic pore conductance G_0 at the voltage amplitude V_0. In Eq. (5), we have introduced the experimental ratio $r = G_+^{\mathrm{i}}/G_+^{\mathrm{f}} = G_-^{\mathrm{f}}/G_-^{\mathrm{i}}$ corresponding to the initial (i) and final (f) limiting conductances observed in Fig. 1 at voltages $V > 0$ (j = +) and $V < 0$ (j = –).

Note also that a capacitive current

$$I_{\mathrm{C}}(t) = C\frac{\mathrm{d}V}{\mathrm{d}t} = CV_0 2\pi f \cos(2\pi f t) \qquad (6)$$

should be added to the conductive currents of Eq. (5) to give the total current. The capacitance C of Eq. (6) can be estimated from the experimental membrane impedance $Z_{V\to 0}$ in the limits of zero voltage and high angular frequency f_{high} as $C 2\pi f_{\mathrm{high}} = 1/Z_{V\to 0}$.[16] For a multipore

membrane with conical nanopores,[16] we have measured $Z_{V\to 0} = 200$ kΩ at f_{high} = 2 kHz. Using the resulting estimation of C in Eq. (6), together with the typical values $f = 20$ s^{-1} and $V_0 = 2$ V, the capacitive current is of the order of 0.1 μA in Eq. (6). Thus, this current is much lower than the conductive current,[6] which is of the order of 10 μA in Fig. 1 and Eq. (6). However, the current of Eq. (7) could still be noted experimentally because of the shift observed in the non-zero crossing point of the I–V curves (Fig. 1).[6,17]

Equations (1)–(6) include the model parameter r together with the frequency ratios f_{+0}/f and f_{-0}/f, which are characteristic of the pore system and the external driving, thus being experimentally accessible. This physical model can provide a qualitative description of the observed I–V curves (Fig. 2) for an experimental reference conductance G_0 = 22 μS (Fig. 1). Note here that the reference current I_0 of Fig. 2(a) is corrected by: (*i*) the factor (V_0/2 V) in Fig. 2(b); (*ii*) the factor $\sqrt{X^2+4c^2}/\sqrt{X^2+4c_0^{\,2}}$, where we have used the Donnan equilibrium equation[9,18] with the reference concentrations $X = c_0$ =100 mM, in Fig. 2(c); and (*iii*) the factor (D_i/D_{K^+}), where $i = K^+$, Na^+, and Li^+, in Fig. 2(d).

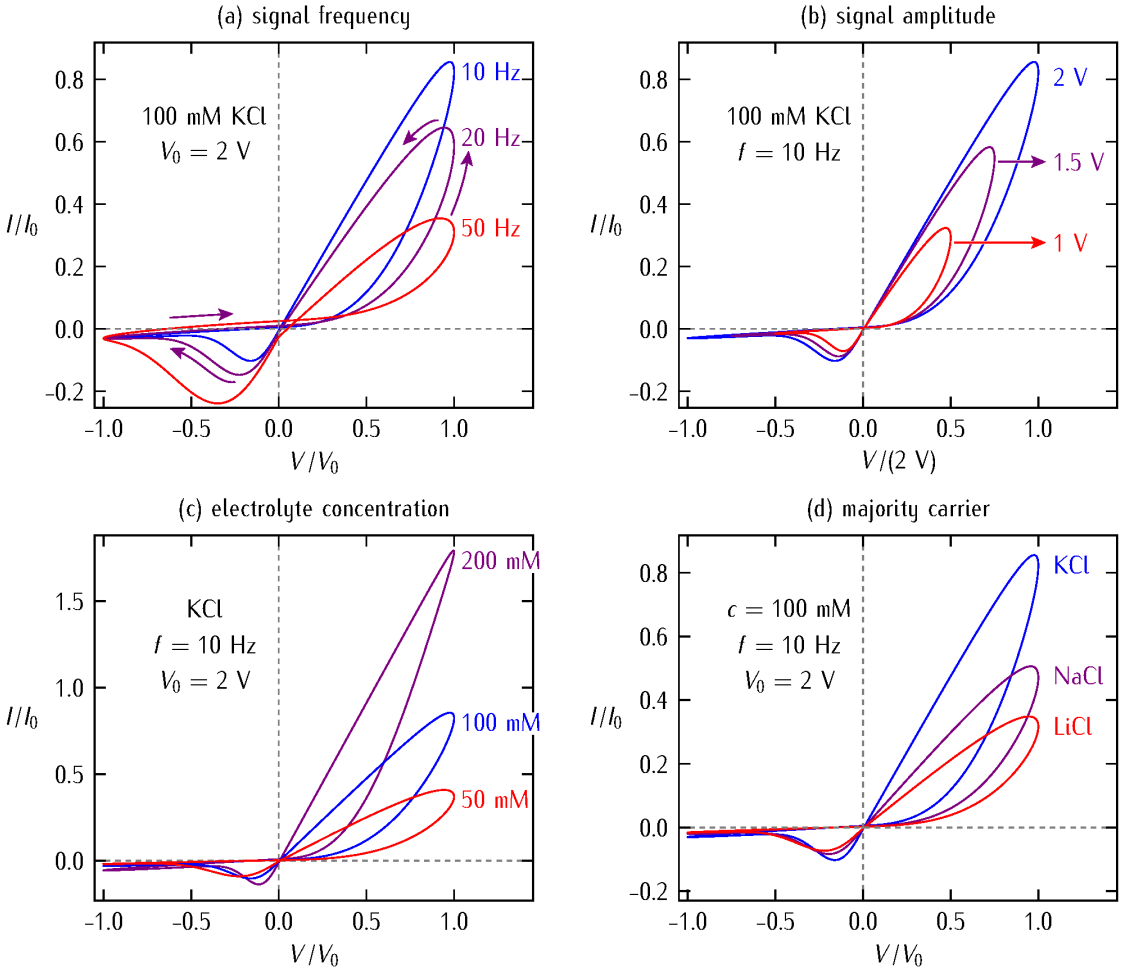

FIG. 2. (a) Theoretical (I/I_0)–(V/V_0) curves for signal frequencies f = 10, 20, and 30 Hz. (b) Theoretical (I/I_0)–$(V/2\text{ V})$ curves for signal amplitudes V_0 = 1.0, 1.5, and 2.0 V. (c) Theoretical (I/I_0)–(V/V_0) curves for ionic concentrations c = 50, 100, and 200 mM. (d) Theoretical (I/I_0)–(V/V_0) curves for different cation diffusion coefficients D. The reference current is $I_0 = G_0V_0$, with V_0 = 2 V and G_0 = 22 μS, and the theoretical parameters are r = 0.03, f_{+0}/f = 3.4π, and f_{-0}/f = 80π. Also, we consider the conductance ratio $C2\pi f/G_0$ = 0.005 with f = 10 Hz to estimate the capacitive current of Eq. (6).

The initial overshooting and subsequent drop of the current $I < 0$ at $V < 0$ can be associated with the following model limitations[9] of Eq. (1): (*i*) when the external concentration

c is of the same order as the reference fixed charge concentration, the coions, which are the electrolyte anions for the negatively-charged pore, may also participate in the pore solution relaxation process of Eq. (1) and (*ii*) both diffusion and conduction may contribute to the total current in this case. Despite the above limitations, the analytical equations do not rely on any numerical procedure and offer a simple and useful description of the applied physics that characterize the nanofluidic pore response. This theoretical description, which can be extended further, is made in terms of experimentally accessible magnitudes such as the driving signal frequency and amplitude, the ionic concentration, and the cation type.

In particular, Figs. 2(c) and 2(d) show that the model captures the effects of the ionic solution characteristics (concentration and cation diffusion coefficient) on the conductances and current rectifications. In particular, the ion accumulation and depletion effects at the pore tip are very significant at low concentration (Fig. 2(c)) because of the decreased Debye screening of the pore surface charges. Also, the observed currents follow the ionic diffusion coefficient series $Li^+ < Na^+ < K^+$ (Fig. 2(d)).

To validate further the above theoretical model, we consider now the experimental *I–V* curves obtained for different pH values of the external solutions (Figs. 3(a) and 3(b)) that modulate the ionization of the pore surface charges.[6,9] The *on*/*off* current states and the *inward/outward* rectifications of Figs. 3(a) and 3(b) can also be observed in the voltage-gated ion channels[12] that regulate *polarized/depolarized* cell membrane potentials along the cell cycle and other biological rhythms.[12,19] Figures 3c and 3d show again that the model results can give a qualitatively description of the experimental data of Figs. 3a and 3b.

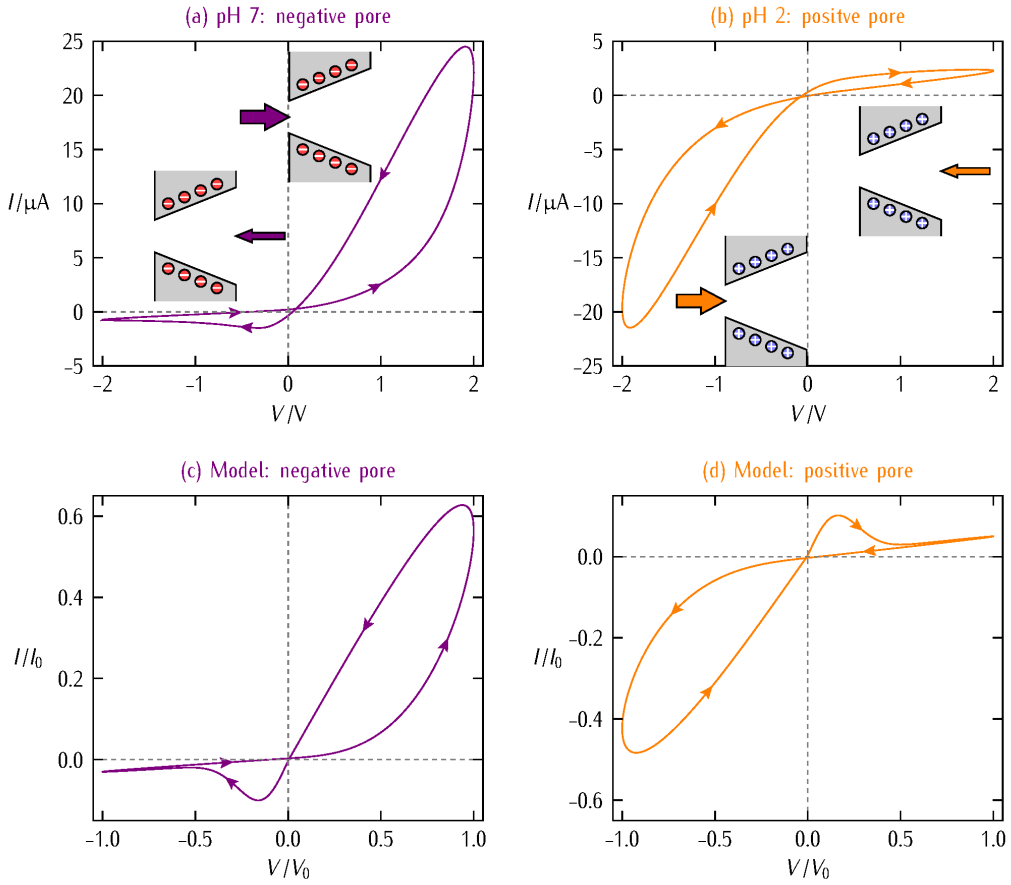

FIG. 3 (a) Experimental *I–V* curve obtained for c = 50 mM KCl, V_0 = 2 V, and f = 20 Hz for a negatively-charged pore (*inset*) corresponding to a neutral pH solution (b) Experimental *I–V* curve for the positively-charged pore corresponding to pH = 2.0. The experimental data were obtained for c = 50 mM KCl, V_0 = 2 V, and f = 20 Hz. Reproduced with permission from J. Phys. Chem. Lett. 14, 10930 (2023). Copyright 2023 American Chemical Society. (c) Theoretical (I/I_0)–(V/V_0) curve obtained with the same reference current $I_0 = G_0V_0$ of Fig. 2 for a negatively-charged pore (neutral pH) and the parameters $r = 0.03$, $f_{+0} / f = 1.6\pi$, and $f_{-0} / f = 80\pi$. (d) Theoretical (I/I_0)–(V/V_0) curve for a positively-charged pore (pH = 2.0) and the parameters $r = 0.05$, $f_{+0} / f = 80\pi$, and $f_{-0} / f = \pi$. In both cases, $C2\pi f/G_0 = 0.003$ for a reference frequency f = 20 Hz. Note that the capacitive current is positive for the negatively-charged pore while it is negative for the positively-charged pore.[6]

Figure 4 gives the theoretical dimensionless conductance (G/G_0) and current (I/I_0) *vs.* dimensionless voltage (V/V_0) plots, obtained for the cases of asymmetric (Figs. 4(a) and 4(b)) and quasi-symmetric (Figs. 4(c) and 4(d)) membranes. As in the cases of Figs. 2 and 3, these theoretical results provide useful physical insights on the applied physics of the nanofluidic pores. Also, Figs. 4(a) and 4(b), which are obtained with the same parameters of Fig. 2, are in qualitative agreement with the experimental results of Fig. 1.

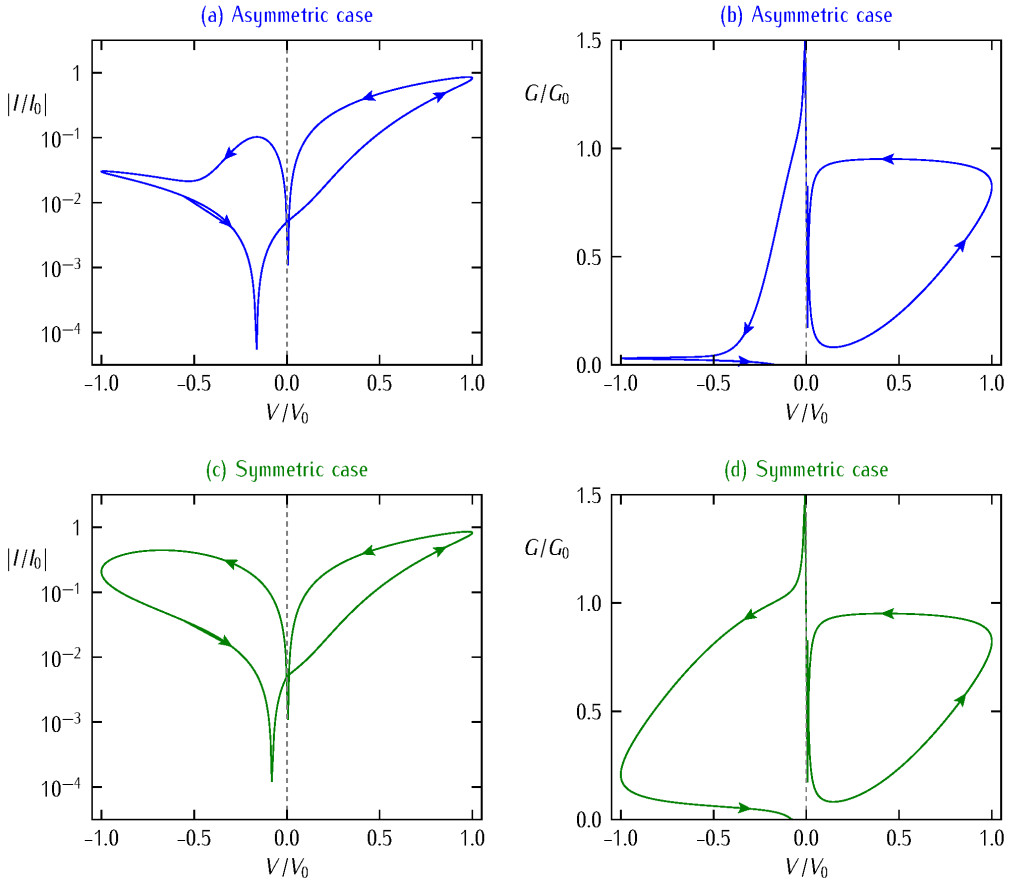

FIG. 4. (a) Theoretical (I/I_0) *vs.* (V/V_0) semi-logarithmic plot for an asymmetric membrane with $r = 0.03$, $f_{+0}/f = 3.4\pi$, and $f_{-0}/f = 80\pi$, with $C2\pi f/G_0 = 0.003$. (b) Theoretical (G/G_0) *vs.* (V/V_0) for the this membrane. (c) Theoretical (I/I_0) *vs.* (V/V_0) semi-logarithmic plot for a

quasi-symmetric membrane with $r = 0.03$, $f_{+0} / f = f_{-0} / f = 3.4\pi$, and $C2\pi f/G_0 = 0.003$. (d) Theoretical (G/G_0) *vs.* (V/V_0) for the this membrane.

III. CONCLUSSION

In conclusion, we have proposed a physical model that accounts for the basic phenomenology observed in memristive asymmetric pores with fixed charges. The model should be a useful addition to the increasing number of devices and experimental data of nanofluidic memory devices. The fundamental concepts invoked describe the nanopore operation on the basis of the electrical interaction between the pore surface charges and the nanoconfined ionic solution. The model is validated by studying the nanofluidic tunability as a function of the amplitude and frequency of the driving signal, the ionic concentration, and the solution pH. The modeling equations can be extended further to other ionic transport phenomena in nanofluidic slits, hybrid soft nanochannels, and finite ion size effects.[20-22] It should also attract interest for the design of electrochemical logic functions and memory circuits.[23-30] In addition, new functionalities could also be explored for the case of divalent and trivalent cations because of the pore charge inversion that occurs when these cations are adsorbed on the negatively charged pore surface.[31,32]

ACKNOWLEDGMENTS

J.C., S.P., P.R., and S.M. acknowledge the support from the *Ministerio de Ciencia e Innovación* (Spain) and the *European Regional Development Funds* (FEDER), project PID2022-139953NB-I00. We are grateful to Juan Bisquert for discussions.

AUTHOR DECLARATIONS

Conflict of Interest

The authors have no conflicts to disclose.

Author Contributions

Javier Cervera: Conceptualization (equal); Formal analysis (equal); Funding acquisition (equal); Investigation (equal); Methodology (equal); Project administration (equal); Writing – review & editing (equal). **Sergio Portillo:** Conceptualization (equal); Formal analysis (equal); Investigation (equal); Methodology (equal); Writing – review & editing (equal). **Patricio Ramirez:** Conceptualization (equal); Formal analysis (equal); Investigation (equal); Methodology (equal); Writing – review & editing (equal). **Salvador Mafe:** Conceptualization (lead); Formal analysis (equal); Funding acquisition (equal); Investigation (equal); Supervision (equal); Writing – original draft (lead).

DATA AVAILABILITY

The data that support the findings of this study are available from the corresponding author upon reasonable request.

REFERENCES

[1]B. Xie, T. Xiong, W. Li, T. Gao, J. Zong, Y. Liu, and P. Yu, "Perspective on Nanofluidic Memristors: From Mechanism to Application," Chem Asian J. **17**, e202200682 (2022).

[2]Y. Hou, Y. Ling, Y. Wang, M. Y. Wang, X. Li, and X. Hou, "Learning from the Brain: Bioinspired Nanofluidics," J. Phys. Chem. Lett. **14**, 2891 (2023).

[3]P. Robin, T. Emmerich, A. Ismail, *et al.* "Long-Term Memory and Synapse-Like Dynamics in Two-Dimensional Nanofluidic Channels," Science **379**, 161 (2023).

[4]T. Xiong, C. Li, X. He, B. Xie, J. Zong, Y. Jiang, W. Ma, F. Wu, J. Fei, P. Yu, and L. Mao, "Neuromorphic functions with a polyelectrolyte-confined fluidic memristor," Science **379**, 156 (2023).

[5]Y. Hou, Y. Ling, Y. Wang, M. Wang, Y. Chen, X. Li, and X. Hou, "Learning from the brain: Bioinspired nanofluidics", J. Phys. Chem. Lett. **14**, 2891 (2023).

[6]P. Ramirez, V. Gomez, J. Cervera, S. Mafe, and J. Bisquert, "Synaptic Tunability of Multipore Nanofluidic Memristors," J. Phys. Chem. Lett. **14**, 10930 (2023).

[7]T. M. Kamsma, W. Boon, Q. T. ter Rele, C. Spitoni, and R. van Roij, "Iontronic Neuromorphic Signaling with Conical Microfluidic Memristors," Phys. Rev. Lett. **130**, 268401 (2023).

[8]J. Bisquert, "Iontronic Nanopore Model for Artificial Neurons: The Requisites of Spiking", J. Phys. Chem. Lett. **14**, 9027−9033 (2023).

[9]J. Cervera, B. Schiedt, R. Neumann, S. Mafe, and P. Ramirez, "Ionic conduction, rectification, and selectivity in single conical nanopores," J. Chem. Phys. **124**, 104706 (2006).

[10]I. Vlassiouk and Z. S. Siwy, "Nanofluidic Diode," Nano Lett. **7**, 552 (2007).

[11]Z. S. Siwy, M. L. Bruening, and S. Howorka, "Nanopores: synergy from DNA sequencing to industrial filtration – small holes with big impact", Chem. Soc. Rev. 52 (2023) 1983−1994.

[12]J. Cervera, M. Levin, and S. Mafe, "Bioelectricity of non-excitable cells and multicellular pattern memories: Biophysical modeling", Phys. Rep. **1004**, 1 (2023).

[13]V. S. Markin, A. G. Volkov, and L. Chua, "An analytical model of memristors in plants", Plant Signal. Behav. **9**, e972887 (2014).

[14]L. O. Chua and K. S. Mo, "Memristive devices and systems," Proc. IEEE **64**, 209 (1976).

[15]Y. V. Pershin and M. Di Ventra, "Memory effects in complex materials and nanoscale systems," Adv. Phys. **60**, 145 (2011).

[16]P. Ramirez, J. Cervera, M. Ali, S. Nasir, W. Ensinger, and S. Mafe, "Electrochemical impedance spectroscopy of membranes with nanofluidic conical pores", J. Colloid Interface Sci. **655**, 876 (2024).

[17]D. Wang, J. Liu, M. Kvetny, Y. Li, W. Brown, and G. Wang, "Physical origin of dynamic ion transport features through single conical nanopores at different bias frequencies", Chem. Sci. **5**, 1827 (2014).

[18]K. Kontturi, L. Murtomäki, J.A. Manzanares, Ionic Transport Processes in Electrochemistry and Membrane Science (Oxford University Press, New York, 2008).

[19]J. R. M. Harvey, A.E. Plante, and A.L. Meredith, "Ion channels controlling circadian rhythms in suprachiasmatic nucleus excitability", Physiol Rev. **100**, 1435 (2020).

[20]P. Robin, N. Kavokine, and L. Bocquet, "Modeling of emergent memory and voltage spiking in ionic transport through angstrom-scale slits", Science **373**, 687 (2021).

[21]A. Heydari, M. Khatibi, and S. Ashrafizadeh, "Fine-tuning ionic transport through hybrid soft nanochannels: The role of polyelectrolyte charge density distribution", Phys. Fluids **35**, 082006 (2023).

[22]D. Pandey and S. Bhattacharyya, "Influence of finite ion size and dielectric decrement on the ion current rectification in a single conical nanopore", Phys. Fluids **33**, 062006 (2021).

[23]M. Ali, P. Ramirez, S. Nasir, J. Cervera, S. Mafe, and W. Ensinger, "Ionic circuitry with nanofluidic diodes," Soft Matter **15**, 9682 (2019).

[24]D. Duleba and R. P. Johnson, "Iontronics: from fundamentals to ion-controlled devices", Curr. Opin. Electrochem. **34**, 100989 (2022).

[25]V. Gomez, P. Ramirez, J. Cervera, M. Ali, S. Nasir, W. Ensinger, and S. Mafe, "Concatenated logic functions using nanofluidic diodes with all-electrical inputs and outputs," Electrochem. Commun. **88**, 52 (2018).

[26]V. Nikonenko and N. Pismenskaya, "Ion and Molecule Transport in Membrane Systems 3.0 and 4.0", Int. J. Mol. Sci., **24**, 8211 (2023).

[27]G. Dou, J. Liu, W. Guo, L. Liu, D. Zhang, and M. Guo, "A liquid electrolyte-based memristor with application in associate learning", Appl. Phys. Lett. **123**, 124102 (2023).

[28]Y. Zhang, Z. Wang, J. Zhu, Y. Yang, M. Rao, W. Song, Y. Zhuo, X. Zhang, M. Cui, L. Shen, R. Huang, and J. J. Yang, "Brain-inspired computing with memristors: Challenges in devices, circuits, and systems," Appl. Phys. Rev. **7**, 011308 (2020).

[29]P. Wang, M. Wang, F. Liu, S. Ding, X. Wang, G. Du, J. Liu, P. Apel, P. Kluth, C. Trautmann, and Y. Wang, "Ultrafast ion sieving using nanoporous polymeric membranes", Nat. Commun. **9**, 569 (2018).

[30]M. Queralt-Martín, M. L. López, M. Aguilella-Arzo, V. M. Aguilella, and A. Alcaraz, "Scaling Behavior of Ionic Transport in Membrane Nanochannels", Nano let. 18, 6604 (2018).

[31]P. Ramirez, J. A. Manzanares, J. Cervera, V. Gomez, M. Ali, S. Nasir, W. Ensinger, S. Mafe, "Surface charge regulation of functionalized conical nanopore conductance by divalent cations and anions", Electrochim. Acta 325, 134914 (2019).

[32]P. Ramirez, J. A. Manzanares, J. Cervera, V. Gomez, M. Ali, I. Pause, W. Ensinger, S. Mafe, "Nanopore charge inversion and current-voltage curves in mixtures of asymmetric electrolytes", J. Membrane Sci. 563 (2018) 633–642.